Multiple Control Plane Joint Operation Method under Overlaid Cell Structure Environment for Future Mobile Communications

Soon-Gi Park, Jun-Sik Kim, Sung-Cheol Jang, Yong-Seouk Choi, Young-Jo Ko
Mobile Communication Research Division
Electronics and Telecommunications Research Institute (ETRI)
Daejeon, Republic of Korea
yoyo@etri.re.kr, junsik@etri.re.kr, scchang@etri.re.kr, choiys@etri.re.kr, koyj@etri.re.kr

***Abstract*—The use of very high frequencies (e.g., THz) in cellular mobile communications results in smaller cell sizes due to significant radio propagation loss, ultimately leading to the formation of ultra-dense networks (UDN). Additionally, due to their ultra-wideband nature, these frequencies are divided into multiple component carriers (CCs) to efficiently utilize the available radio resources. Applying carrier aggregation (CA) technology to these CCs enables high-capacity data transmission. However, the performance at the cell edge can be severely degraded or subject to significant variations. To address this issue, technologies such as coordinated multi-point (CoMP) or dual active protocol stack (DAPS) have been introduced, enabling some improvements in user plane (UP) performance. Nevertheless, when considering ultra-high-speed user equipment (UE) or UDN environments, it is still essential to consider cell-edge performance improvements not only on the UP side but also on the control plane (CP) side. In this paper, we assume an overlaid cell structure (OCS) environment where individual layer cell groups are established, allowing ensuring that cell edges between layers do not overlap and specific master nodes (MNs) to move within specific layers. Additionally, we propose the multiple control plane joint operation (MCPJO) method, which utilizes two or more control planes and wireless connectivity with two or more master nodes. This environment and method offer significant improvements in cell-edge performance by reducing fluctuations in user capacity and enhancing handover movement stability.**

Keywords—Multiple Control Plane, Overlaid Cell Structure, Ultra-Dense Network, Dual Steering, Carrier Aggregation

I. INTRODUCTION

Given the ongoing rapid increase in the number of mobile devices and the emergence of new ultra-high-capacity, ultra-high-reliability, and ultra-low-latency applications in the future [1], continuous research is needed to meet the new requirements related to them. Generally, to increase mobile capacity, there are methods such as using new frequency bands, improving frequency utilization efficiency, and increasing network density [2,3]. The introduction of mmWave bands in 5G, expanding up to 100 GHz, and the expected inclusion of THz bands in future 6G are examples of such advancements. The use of these high and ultra-high frequencies inevitably leads to the formation of ultra-dense networks (UDN) due to their propagation characteristics. In UDNs utilizing these frequency bands, new or evolved technologies are required to overcome the performance degradation at the cell edge while ensuring an adequate level of user equipment (UE) capacity and area capacity. In this context, this paper proposes the multiple control plane joint operation (MCPJO) method in the overlaid cell structure (OCS or ocs) environment and presents performance improvements through various simulation results.

II. BACKGROUND

As shown in Fig. 1 [4-6], the 3rd Generation Partnership Project (3GPP) adheres to the principle of having a single control plane (CP) on the UE (User Equipment)-MN (Master Node) A-CN (Core Network) path, and it consists of two control interfaces: the RAN (MN A)-UE control interface and the RAN (MN A)-CN control interface (e.g., S1-C in 4G, NG-C in 5G). After this basic configuration, to increase wireless capacity, MN A secondary cells (SCells) may be associated with MN A primary cell (PCell) through carrier aggregation (CA or ca). Additionally, if the UE is located within the coverage of the Secondary Node (SN A), to offload the radio capacity of MN A to SN A, the SN A primary secondary cell (PSCell) is linked to MN A PCell through dual connectivity (DC or dc). Subsequently, SN A SCells may be associated with SN A PSCell through CA. Consequently, MN A PCell serves as the basis of MN A SCells in CA and the reference point of SN A (PSCell) in DC simultaneously, where only MN A PCell is the reference point for mobility management (inter-cell mobility). The single CP operation mechanism of 3GPP (the configuration shown on the right side of Fig. 1) may cause some problems, as depicted in Fig. 2. If PCell re-selection occurs due to various factors (handover failure (HOF), radio link failure (RLF), beam failure (BF), etc.), the radio capacity supported by the above-mentioned overall configuration (MN PCell, MN SCells, and/or SN PSCell/SCells) cannot be utilized during the period required for PCell recovery and the subsequent addition of component carriers (CCs) available in MN/SN. Hence, as the data rate increases, the instability of PCell's radio connectivity has more adverse effects on the uniform QoS and packet transmission delay and packet loss. When transmitting very large amounts of data, it may be necessary to prepare a substantial buffer to prevent packet loss (e.g., a 125-gigabyte buffer for 1 second at 1 Tbps). However, even if the packet loss is mitigated, the resulting packet delay and data rate fluctuation are unavoidable. When PCell uses mmWave or THz, PCell re-establishment due to blockage and deafness occurs even more rapidly and frequently. Due to this PCell re-selection and the subsequent

MN CA and SN DC/CA related procedures, it is difficult for the single CP operation mechanism of 3GPP to support uniform QoS in the existing and new radio environments (UDN, the use of mmWave or THz PCell, the uniform ultra-high data rate requirements in new services such as extended reality (XR)).

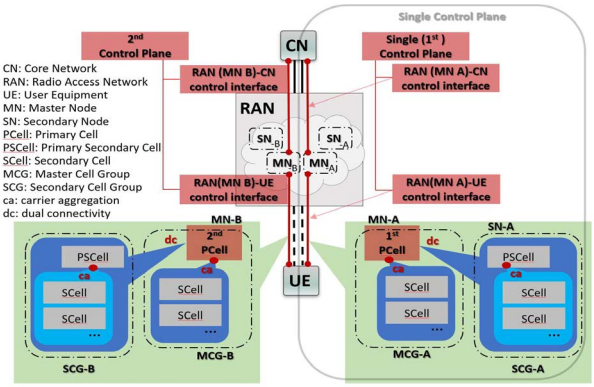

Fig. 1. Single and multiple control plane operation mechanism.

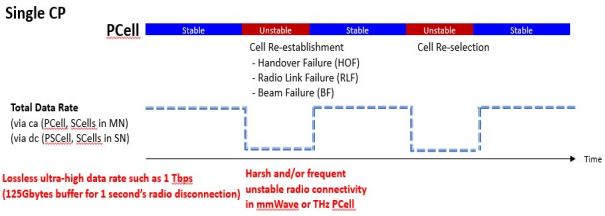

Fig. 2. The QoS support in single CP operation situation.

III. Wayforward and MCPJO

3GPP coordinated multi-point (CoMP) or dual active protocol stack (DAPS) or further enhanced MIMO (feMIMO) inter-cell beam management (ICBM) or conditional handover (CHO) may improve some performances on the user plane (UP) or CP, (e.g., data rate and transmission reliability or mobility robustness enhancement). In the further NR mobility enhancement work item in 3GPP radio access network (RAN) 2 and 3, L1/L2-based mobility is being studied to provide the inter-cell mobility faster than the existing L3-based one, but its application may be limited to intra-base station (e.g., intra-distributed unit (DU), inter-DU and inter-sector within one base station). However, the effect of guaranteeing uniform QoS at any location in the cell through CoMP, DAPS, feMIMO ICBM, CHO, and L1/L2-based mobility is very insignificant in the case of frequent change and re-selection situation of PCell (e.g., UE moving in UDN). From a longer-term perspective, there may be two technologies: cell free massive multiple-input multiple-output (CFmMIMO) and MCPJO, as discussed in this paper. CFmMIMO is a technology that combines the advantages of UDN with cellular mMIMO to increase system capacity and improve cell edge capacity [7][8]. In contrast, MCPJO, as shown in Fig. 1, is a method that aims to achieve two benefits (system and cell-edge capacity) simultaneously in both existing and new radio environments while retaining the existing cell concept. The core concept of MCPJO is to operate multiple PCells (1st PCell and 2nd PCell in Fig. 1). It is assumed that each PCell should have an independent CN-RAN control interface, and the CN should accommodate independent NAS signaling (e.g., attach/detach, etc.) per PCell for the same UE. In Fig. 3, it is assumed that two PCells operate at different coverage layers, and that each PCell may experience repeated unstable and stable states. Joint operations (packet switching (ps), packet balancing (pb), and packet duplication (pd)) are performed in such states. The ps decision in joint operations can reduce packet transmission delay, packet interruption time, and packet loss. Additionally, the pb can increase the data rate, and the pd can improve the reliability of data transmission. Here, the capacity cells available in the capacity layer (MN SCells and/or SN PSCell/SCells) may belong to two PCells independently or overlap. In other words, the same capacity cells may or may not be associated with two PCells at the same time. The detailed joint operations can be selected for each QoS flow or each group of QoS flows through comprehensive considerations, including the radio status of multiple PCells and all capacity cells related to them. Although the introduction of MCPJO clearly increases network complexity, it can greatly help achieve uniform QoS and enhance cell edge performance in UDN, utilizing the existing and (very-) high frequencies in the future. The MCPJO concept can be designed in two types, based on where the decision authority of the joint operations (ps, pb, and pd) is located, either in the CN or any one of the MNs. Commonly, the CN can manage an independent CN-RAN control interface (e.g., NG-C) for each PCell of one UE, and it should support enabling independent NAS signaling for each control interface. All procedures in each MCPJO method are divided into two stages: MCPJO preparation and MCPJO execution. The first stage (preparation) involves preparing for the MCPJO execution stage, and the second stage (execution) is the process of determining and executing joint operations.

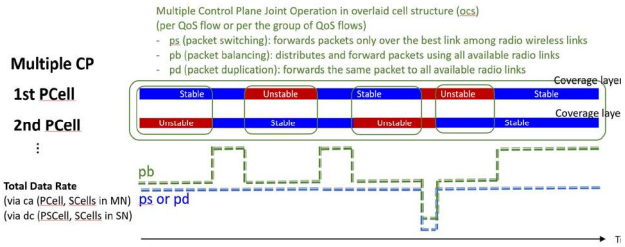

Fig. 3. The QoS support in multiple CP operation situation.

IV. Simulation Setup and Results

A. Simulation Setup

As the current 5G NS-3 network simulator [10] has been built in the form of adding an mmWave channel and implementing its PHY/MAC based on the 4G NS-3 source [9], simulating a 6G network will be possible in a similar way as well. Although it is possible to import the THz propagation path loss and molecular absorption module of TeraSim NS-3 source [11] to the 4G and 5G NS-3 framework, it is still difficult to perform a 6G THz network simulation because the

current 5G NS-3 source is still in the process of being completed [12], and there is no consensus about both 6G numerology and its basic operation. Fortunately, the proposed MCPJO can be implemented in 4G NS-3, and its performance results can be obtained in this paper. Through them, the MCPJO's performance in the 5G/6G environment can be predicted to some extent.

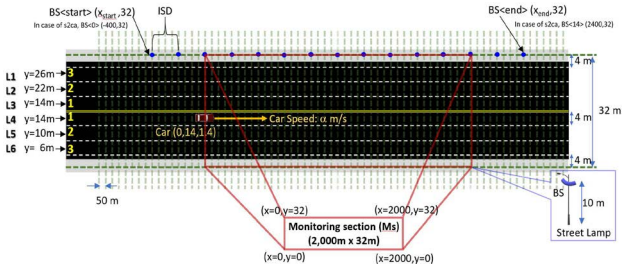

Fig. 4. The road environment for MCPJO performance test.

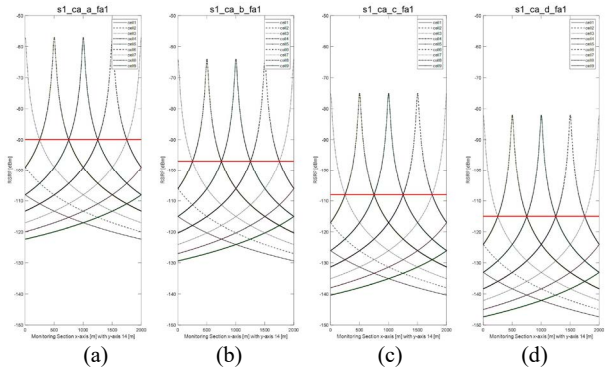

Fig. 5. Four CRS power levels in s1 ca fa1.

For the MCPJO performance test, we prepared the road environment as shown in Fig. 4 and specified in Table I, while using the system parameters listed in Table II. The road environment consists of a six-lane road (L1~L6), with base stations (sites) arranged along the upper side of the road. Table I shows the details of two environments: s2ca and s2ocs. The s2ca environment comprises 15 sites (i.e., BS<0> thru BS<14>), with two cells per site (cell-fa1, cell-fa2), resulting in a total of 30 cells (15 sites x 2 cells). On the other hand, the s2ocs environment also has 15 sites, but the cells are created differently. If the number in the angle brackets of

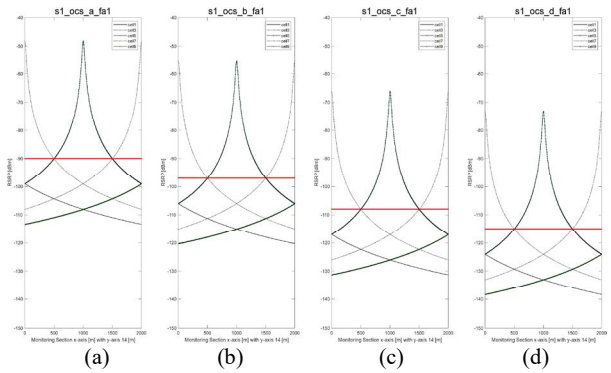

Fig. 6. Four CRS power levels in s1 ocs fa1.

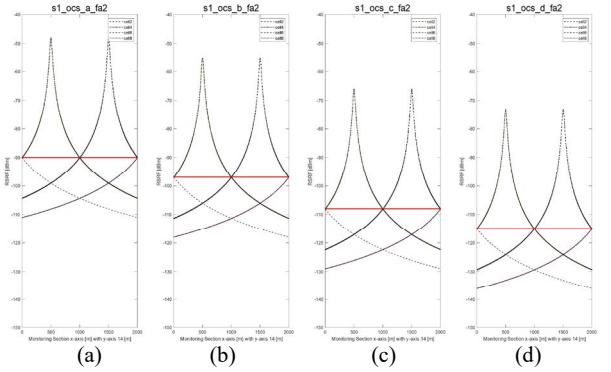

Fig. 7. Four CRS power levels in s3 ocs fa2.

BS (i.e., BS<>) is even, the cells are made using fa1 frequency (8 cells), and if the number is odd, the cells are created using fa2 frequency (7 cells), totaling 15 cells. Additionally, as the right number (i.e., s1, s2, s3, s4) of the 's' character increases, the inter-site distance (ISD) decreases (i.e., 500, 200, 100, 50), resulting in a denser cell network. The cell transmission (Tx) powers are set to meet the four CRS crossing levels of Table II (a: excellent -90, b: good -97, c: fair -108, d: poor -115) between two cells with the same frequency (e.g., Fig. 5, Fig. 6, and Fig. 7). Performance results fall into two categories: one for multiple UE performance and the other for single UE performance. The commonality of the two performance tests is obtained within the monitoring section (Ms) of Fig. 4, and the difference lies in whether the UE moves or not (e.g., UE speed 0m/s or 20m/s). In the former case, there is one simulation placing 24

TABLE I. SCENARIO (CA AND OCS) AND BS/CELL CONSTITUTION

Scenario	BS<start>	~ BS<end>	Site No.	ISD [m]	start x-axis [m]	end x-axis [m]	Cell Dia. [m]	Cell No.	Cell No. joining in Ms	BS <No.> DL EARFCN
s1ca	<0>	<8>	9	500	-1000	3000	500	18	10 (8)	<all> 2500 & 3200
s2ca	<0>	<14>	15	200	-400	2400	200	30	22 (20)	<all> 2500 & 3200
s3ca	<0>	<24>	25	100	-200	2200	100	50	42 (40)	<all> 2500 & 3200
s4ca	<0>	<44>	45	50	-100	2100	50	90	82 (80)	<all> 2500 & 3200
s1ocs	<0>	<8>	9	500	-1000	3000	1000	9	5 (4)	<even> 2500, <odd> 3200
s2ocs	<0>	<14>	15	200	-400	2400	400	15	11 (10)	<even> 2500, <odd> 3200
s3ocs	<0>	<24>	25	100	-200	2200	200	25	21 (20)	<even> 2500, <odd> 3200
s4ocs	<0>	<44>	45	50	-100	2100	100	45	41 (40)	<even> 2500, <odd> 3200

ca: carrier aggregation, ocs: overlaid cell structure, BS: Base Station, ISD: Inter Site Distance, DL: Downlink, EARFCN: EUTRA Absolute Radio Frequency Channel Number

TABLE II. SIMULATION PARAMETERS

Parameter	Value
Total Bandwidth	10 MHz
Carrier Frequency	fa1 EARFCN DL 2500
	fa2 EARFCN DL 3200
	In case of EARFCN UL = DL EARFCN + 18000
Resource Bandwidth	180 kHz
Number of RBs	50
Transmission Time Interval (TTI)	1 ms
CRS Crossing Power Level (RSRP)	a (excellent): -90 dBm, b (good): -97 dBm, c (fair): -108 dBm, d (poor): -115 dBm
Number of UEs (Cars)	Single UE 1 EA
	Multiple UE 24 EA/Cell
UE (Car) Speed	Multiple UE 0 km/s (0 m/s)
	Single UE 72 km/h (20 m/s)
Traffic Type	UDP

CRS: Cell-specific Reference Signal, RSRP: Reference Signals Received Power

UEs per cell randomly based on the fa1 cell, and their performances (Ms Capacity, Ms UE Cell Edge Capacity, Ms UE Capacity, and Ms UE Capacity standard deviation (Std)) are obtained through N simulations, each of which converges to a certain value (two RBs are allocated per one UE). The latter aims to obtain the data rate over distance when driving at the UE speed of 20 m/s at distances ranging from 0 to 2000 m along the x-axis in the fourth lane (L4) (48 RBs are allocated to a single UE). Fig. 5 shows CRS RSRP quality over the distance ((a), (b), (c), (d)) according to the four CRS cross power levels (a, b, c, d) for frequency fa1, in the situation where the UE moves from 0 m to 2000 m on the x-axis of L4 within Ms under the s1_ca environment of Table I. For the fa2 cells, the four graphs for RSRP over distance according to the four power levels are almost identical to Fig. 5 because it creates one fa2 cell at the same location as one fa1 cell. Hence, there are a total of 18 cells with a cell diameter of 500 m in s1_ca (9 cells on fa1 (cell1 thru cell9) plus 9 cells on fa2 (cell1a thru cell9a), i.e., Cell No. in s1_ca of Table I: 18). In Fig. 5, the number of fa1 cells that the UE can use for service within Ms is a total of 5 (cell3, cell4, cell5, cell6, cell7), but there are two cells (cell3, cell7) located on the Ms boundary and containing only half coverage. So, if these two are treated as one cell, the number of effective fa1 cells participating in Ms is 4 in total. Similarly, the number of fa2 cells participating actually or effectively in Ms is 5 or 4, respectively. As a result, the number of cells joining actually or effectively in Ms is 10 or 8, respectively, in the s1_ca environment (Cell No. joining in Ms of Table I s1ca is expressed as 10(8)). Similar to what was described previously, Fig. 6 and Fig. 7 show RSRP over distance for fa1 cells and fa2 cells, respectively, in the s1_ocs environment. Here, there are a total of 9 cells (cell1/3/5/7/9 using fa1 plus cell2/4/6/8 using fa2), and there are a total of 5 or 4 cells (Cell Dia. 1000 m) that actually or effectively join in the Ms (i.e., 3 cells (cell3, cell5, cell7) formed by fa1 and 2 cells (cell4, cell6) formed by fa2, 2 cells (cell3, cell7) located in the Ms boundary). Considering the 'Cell Dia.' and 'Cell No. joining in Ms' of Table I (that is, when the same cell size and the number of effective cells in parentheses participating in Ms are the same), it may be reasonable to compare performance with s2_ca versus s3_ocs and s3_ca versus s4_ocs.

B. Results

Fig. 8 to 12 show multiple UE performances, and Fig. 13 to 15 show single UE performances (data rate over distance, unit: Mbps). Fig. 8 shows Ms Capacity (unit: Mbps), which is defined as the capacity provided in the Ms area by an environment (e.g., s2_ca_b or s3_ocs_b, where "b" denotes the CRS crossing power level). Fig. 9 represents Ms UE Cell Edge Capacity (average for the lower 5% of UE capacity, unit: Mbps). Fig. 10 displays Ms UE Capacity (average UE capacity, unit: Mbps). Fig. 11 illustrates Ms UE Capacity Std. (standard deviation of UE capacity, unit: Mbps), and Fig. 12 represents the probability of a UE having a data rate of 0 (also known as Non-Served UE probability, unit: %). The difference between ocs_ps and ocs_pb lies in whether data transmission is performed using only one cell (ps) with better radio quality among two cells (fa1 cell and fa2 cell) in an overlapping cell structure (ocs), or using both (pb) simultaneously. The ocs_ps can be considered somewhat similar to the conventional single CP operation as it selects only one cell for data transmission. Here, the performance results of ocs_ps can be seen as demonstrating the advantages that can be obtained through ocs, and the ocs_pb performance results can be seen as representing the benefits resulting from both ocs and the MCPJO approach.

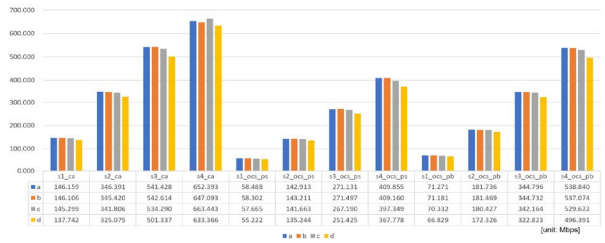

Fig. 8. Ms Capacity.

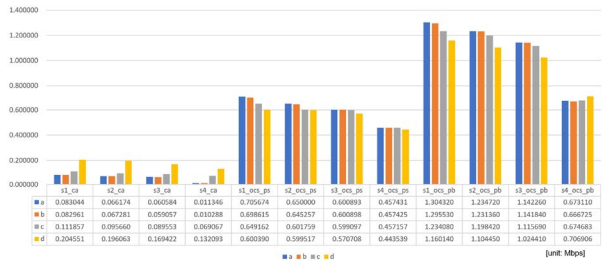

Fig. 9. Ms UE Cell Edge Capacity.

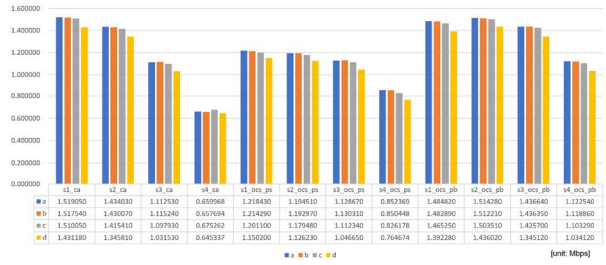

Fig. 10. Ms UE Capacity.

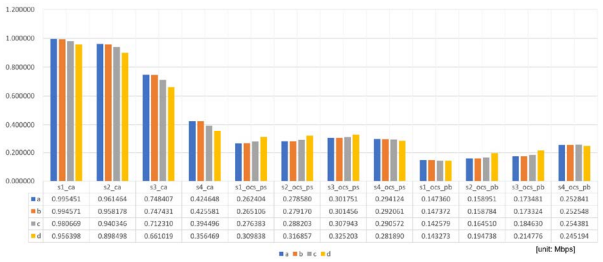

Fig. 11. Ms UE Capacity Standard Deviation (Std.).

In all cases (ca, ocs_ps, ocs_pb) of Fig. 8, Ms Capacity generally tends to improve as the network becomes denser (s1->s2->s3->s4, indicating that the more cells there are in Ms). When comparing s2_ca and s3_ocs_pb (or s3_ca and s4_ocs_pb) under the same conditions (the cell diameter and the effective number of cells joining in Ms), there is no significant difference in Ms Capacity (e.g., in case a: 346.391 Mbps vs. 344.796 Mbps (or 541.428 Mbps vs. 538.840), and in case c: 341.806 Mbps vs. 342.164 Mbps (or 534.290 Mbps vs. 529.622 Mbps)). Regarding Ms UE Cell Edge Capacity in Fig. 9, ca results show poor performance in all network topologies (s1, s2, s3, s4). However, ocs_ps (i.e., stand-alone ocs environment) performs better than ca, and the best performance is achieved by performing pb operation in ocs together (i.e., ocs_pb). When comparing s3_ocs_pb based on s2_ca and s4_ocs_pb based on s3_ca, a significant performance improvement can be observed with an increase of +1166% (c: 1.115690 based on 0.095660 Mbps) and +535% (d: 0.706906 based on 0.132093 Mbps). As the network becomes denser, Ms Capacity tends to increase, whereas Ms Cell Edge Capacity tends to deteriorate in ocs_ps/pb due to the increase in inter-cell interference. In Fig. 10 and Fig. 11, both Ms UE Capacity and its fluctuations (Ms UE Capacity Std.) decrease in ca as the network becomes denser. When comparing s2/3_ca_a/b/c/d based on s3/4_ocs_pb_a/b/c/d, respectively, Ms UE Capacity (Fig. 10) showed almost the same values, ranging from -0.05% to +0.90%. Ms Capacity (Fig. 8) exhibited a capacity difference from -1.02% to +0.10%. Ms UE Cell Edge Capacity (Fig. 9) showed a capacity difference from +317.25% to +1626.14% (i.e., 317.25=(0.706906 (s4, ocs_pb, d)/0.169422 (s3, ca, d)-1)x100 to 1626.14=(1.142260 (s3, ocs_pb, a)/0.066174 (s2, ca, a)-1)x100), and Ms UE Capacity Std. (Fig. 11) showed a

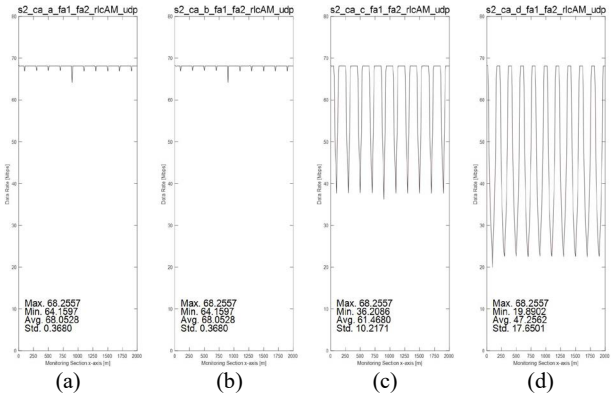

Fig. 12. The data rate on four CRS power levels in s2 ca.

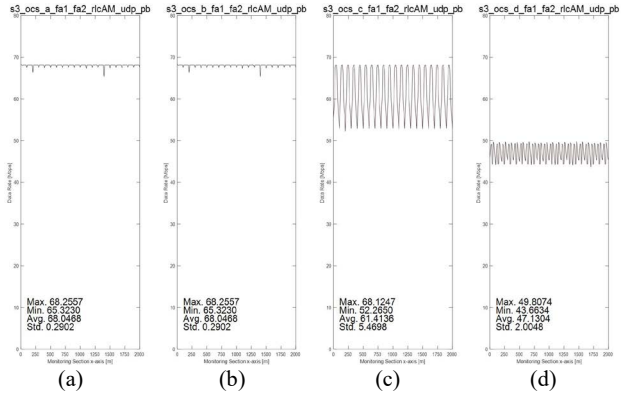

Fig. 13. The data rate on four CRS power levels in s3 ocs pb.

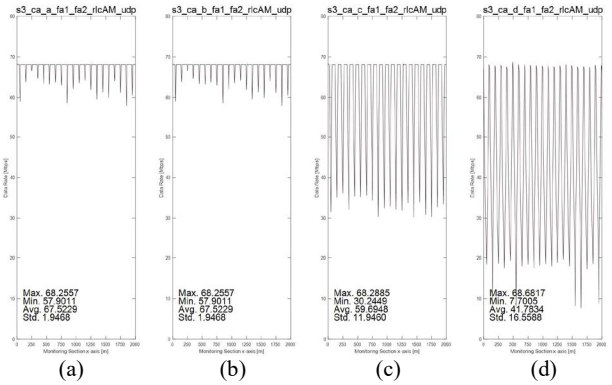

Fig. 14. The data rate on four CRS power levels in s3 ca.

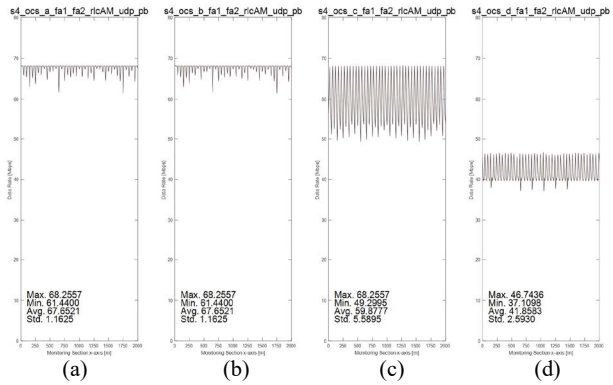

Fig. 15. The data rate on four CRS power levels in s4 ocs pb.

difference of -62.91% to -81.96%. In other words, ocs_pb exhibits a significant cell edge performance improvement and a small capacity variance reduction according to the location of the UE, while providing almost the same Ms Capacity and Ms UE Capacity compared to ca.

In Fig. 12, the data rate results at high powers (a, b) exhibit the same level of performance (Max., Min., Avg., Std.), and they decrease as the power decreases at low powers (c, d), leading to increased fluctuations and forming deep valleys. When comparing ocs_pb of Fig. 13 based on the ca of Fig. 12, the performances of ocs_pb a (or b) are almost the same as those of ca a (or b) (a Max. 0.00%, a Min. +1.81%, a Avg. -0.01%), showing a performance improvement of -21.14% in Std. The ocs_pb c performances show two similar results (c

Max. -0.19%, c Avg. -0.09%), while the rest show clear improvements (c Min. +44.34%, c Std. -46.46%) compared to ca c. Ocs_pb d exhibits a large decrease of -27.03% in Max. and a slight decrease of -0.27% in Avg. compared to ca d, but it also shows two performance improvements (Min. +119.52% and Std. -88.64%). Similarly, when comparing ocs_pb of Fig. 15 based on the ca of Fig. 14, the performances of ocs a (or b) are almost the same as those of ca a (b) (Max. 0.00%, Min. +6.11%, Avg. +0.18%), showing a performance improvement of -40.29% in Std. The ocs_pb c performances show two similar results (Max. -0.05%, Avg. +0.31%), while the rest show clear improvements (Min. +63.00%, Std. -53.21%) compared to ocs c. Ocs_pb d exhibits a large decrease of -31.94% in Max. and a slight increase of +0.18% in Avg., and there are two performance improvements (Min. +381.91% and Std. -84.34%) compared to ca d. If we consider single UE performance, there are almost no performance differences between ca and ocs_pb, but ca shows a rather large data rate variation (Std.) at high powers (a or b). Additionally, there are some performance differences between ca and ocs_pb at low power (c or d), where Avg. is almost the same, but ocs_pb is superior in both Min. and Std. Furthermore, ca and ocs_pb show similar results in c Max., but ca performs better in d Max.

V. CONCLUSION

Considering the usage of mmWave in 5G as well as THz in the future 6G, their cell configurations are bound to become denser networks with much smaller cell sizes, and the number of usable component carriers will become very large. In this paper, we propose the MCPJO method in the OCS environment to address the problems that arise when using only carrier aggregation based on the single control plane principle in a dense network. In terms of multiple UE performances, the CA performances show that Ms Capacity increases, Ms UE Capacity becomes smaller, and Ms UE Cell Edge Capacity is in a very poor situation as the network becomes denser. Regarding single UE performances, the CA performances indicate that the average data rate (Avg.) becomes smaller, and its variance (Std.) becomes rather large. In other words, CA is a powerful means to increase area capacity (i.e., Ms Capacity or system capacity), but it has the disadvantage of very poor cell edge capacity. It may not be suitable for an application service requiring a constant data rate due to the large capacity variance depending on UE location. However, in both multiple and single UE performances applying MCPJO in the OCS environment, it is possible to improve UE Capacity and UE Capacity Std. while providing almost the same area capacity as CA. MCPJO can greatly compensate for the poor cell edge capacity of CA, making it more suitable for applications requiring a fixed data rate.

In conclusion, due to the usage of mmWave and THz, there are many component carriers, some of which can be used for carrier aggregation (CA), while others can also be utilized for the MCPJO method in the OCS environment. Considering these OCS environment configurations and MCPJO operation, it is possible to significantly improve cell edge capacity through appropriate cell transmission power control, and even with loose power settings causing coverage holes within the same layer, continuous and stable data streaming is achievable.

ACKNOWLEDGMENT

This work was supported by Institute of Information & communications Technology Planning & Evaluation (IITP) grant funded by the Korea government (MSIT) (No.2021-0-00746, Development of Tbps wireless communication technology).

REFERENCES

[1] ETRI, 6G Insight Vision and Technologies, Visions, ISBN 978-89-5519-291-9 (November 2020).

[2] M.K. Weldon, The Future X Network: A Bell Labs Perspective, CRC Press, 2016.

[3] T.L. Marzetta, Fundamentals of Massive MIMO, Cambridge Univ. Press, 2016.

[4] 3GPP TR 37.340, E-UTRA and NR; Multi-connectivity; Stage 2, V.16.7.0 (September 2021).

[5] 3GPP TR 38.300, NR and NG-RAN Overall Description; State 2, V16.6.0 (June 2021).

[6] 3GPP TR 36.300, E-UTRA and E-UTRAN; Overall Description; State 2, V16.6.0 (June 2021).

[7] O. T. Demir, E. Bjornson, and L. Sanguinetti, "Foundations of user-centric cell-free massive MIMO," Foundations and Trends® in Signal Processing, vol. 14, no. 3-4, 2021, pp. 162–472.

[8] H. Q. Ngo, A. Ashikhmin, H. Yang, E. G. Larsson, and T. L. Marzetta, "Cell-free massive MIMO: Uniformly great service for everyone," in Proc. IEEE SPAWC, 2015, pp. 201–205.

[9] NS-3 Network Simulator [Online]. https://www.nsnam/org

[10] M. Mezzavilla, M. Zhang, M. Polese, R. Ford, S. Dutta, S. Rangan, M. Zorzi, End-to-End Simulation of 5G mmWave Networks, in: 2018 IEEE Communications Surveys & Tutorials, 2018, Vol., 20, Issue 3, pp. 2237-2263.

[11] Z. Hossain, Q. Xia, J. M. Jornet, TeraSim: An ns-3 extension to simulate Terahertz-band communication networks, in: 2018 ELSEVIER Nano Communication Networks, 2018, Vol., 17, pp. 36-44.

[12] 5G-LENA Simulator [Online]. https://5g-lena.cttc.es

[13] S.G. Park, Dae-Young Kim, Downlink Multi-Point Transmission Effect Using Aggregate Base Station Architecture, IEICE Transactions on Communications, v.E94.B no.12, pp.3374-3377.

[14] S.G. Park, J.S. Kim, Multi-Band/Tier/Space Dynamic Clustering and Transferable Cell Communication assuming High Frequency-Ultra Bandwidth on Road Environment, International Conference on Information and Communication Technology Convergence (ICTC) 2019, pp.870-875.

[15] H.S. Park, Y. Lee, T.J. Kim, B.C. Kim, J.Y. Lee, ZEUS: Handover algorithm for 5G to achieve zero handover failure, ETRI Journal (2022), v.44 no.3, pp.361-378.

[16] H. Kim, S. Baek, Performance analysis of large-scale MIMO system for wireless backhaul network, ETRI Journal (2018), v.40 no.5, pp.582-591.

[17] S.N.K. Marwat, S. Meyer, T. Weerawardane, C. Goerg, Congestion-Aware Handover in LTE Systems for Load Balancing in Transport Network, ETRI Journal (2014), v.36 no.5, pp.761-771.

[18] H.S. Park, Y.S. Choi, B.C. Kim, J.Y. Lee, LTE Mobility Enhancements for Evolution into 5G, ETRI Journal (2015), v.37 no.6, pp.1065-1076.

[19] C. Yeh, G.D. Jo, Y.J. Ko, H.K. Chung, Perspectives on 6G Wireless Communications, ICT Express (tbd) (2022), pp.1-10.

[20] S.E. Hong, On the effect of shadowing correlation and pilot assignment on hybrid precoding performance for cell-free mmWave massive MIMO UDN System, ICT Express 7 (2021), pp.60-70.